Arabian Journal of Geosciences (2021) 14:820
https://doi.org/10.1007/s12517-021-07155-7

ORIGINAL PAPER

Using reflectance spectroscopy and Advanced Spaceborne Thermal Emission and Reflection Radiometer data to identify bauxite deposits in vicinity of Az Zabirah, northern Saudi Arabia

Habes Ghrefat[1] · Yasir Al Mutairi[2] · Hesham ElAraby[1,3] · Mahmoud Galmed[1,4] · Essam Mohamed[1]

Received: 30 December 2020 / Accepted: 23 April 2021

Abstract
Bauxite samples from deposits in northern Saudi Arabia were identified in the laboratory using spectral reflectance measurements (at 0.3–2.5 μm) and X-ray diffraction (XRD). The XRD results revealed that the bauxite deposits are composed mainly of goethite, gibbsite, and boehmite with small amounts of kaolinite, hematite, and quartz. The bauxite spectra revealed the presence of significant iron oxides (at 0.5 and 0.87 μm) accompanied by water (at 1.4 and 1.9 μm) and aluminum hydroxide (at 2.2 μm). The convolved Advanced Spaceborne Thermal Emission and Reflection Radiometer (ASTER) spectra of the bauxite samples were characterized by an aluminum hydroxide feature in ASTER band 6 (at 2.2 μm). The results demonstrated that principal components analysis band PC2 is the best component for delineating the bauxite deposits. Fractional abundances of bauxite were derived by using a matched-filtering method. This study demonstrates the applicability of reflectance spectroscopy and ASTER data to provide spectral information for distinguishing economically important minerals from visible and near-infrared and shortwave-infrared spectra in arid and semiarid environments such as in Saudi Arabia.

Keywords Bauxite · Spectroscopy · Reflectance · Mineralogy · Saudi Arabia

Introduction

Bauxite is composed of a mixture of the aluminum hydroxides gibbsite ($Al(OH)_3$), boehmite (AlO(OH)), and diaspore (AlO(OH)) and the iron oxides goethite (FeO(OH) and hematite (Fe_2O_3), along with kaolinite clay and small amounts of titanium dioxide. Magnetite, siderite, brookite, halloysite, and quartz are also commonly found in bauxite (Valeton 1972; Fahad et al. 2009; Kusuma et al. 2012). Bauxite is formed by intense leaching in tropical and subtropical regions by a process called laterization. Bauxite has many common uses, including as an abrasive, in cement, as a refractory, and in the chemical and metallurgical industries (Kusuma et al. 2012); ~85% of the bauxite produced worldwide is processed into aluminum.

Characterization and identification of some pure mineral species has been successfully accomplished using reflectance spectroscopy based on the minerals' absorption features in the visible and near-infrared (VNIR) and shortwave-infrared (SWIR) wavelength regions (0.4–2.5 μm) (Clark 1999; Thompson et al. 1999; Clark 2011; Rao et al. 2017; Kumar et al. 2018). Several researchers have successfully used reflectance spectroscopy to identify iron oxides and hydroxides, carbonates (CO_3), and sulfates (SO_4). The typical cationic transitional vibrations in phyllosilicates (e.g., –OH-, Al–OH-, Mg–OH-, and Fe–OH-bearing clay, mica, and serpentine) have also been identified by using this method (Grove et al. 1995; Thompson et al. 1999; Chang et al. 2001). In contrast, spectroscopy has been used in only a limited way to distinguish different rock types. Mapping the spatial distribution of the surface exposures of economically important rocks is important when trying to determine the best areas

Responsible Editor: Biswajeet Pradhan

✉ Habes Ghrefat
habes@ksu.edu.sa

[1] Department of Geology and Geophysics, College of Science, King Saud University, Riyadh, Saudi Arabia

[2] King Abdulaziz City for Science and Technology, Riyadh, Saudi Arabia

[3] Geophysics Department, Faculty of Science, Cairo University, Cairo, Egypt

[4] Geology Department, Faculty of Science, Cairo University, Giza, Egypt

Published online: 04 May 2021

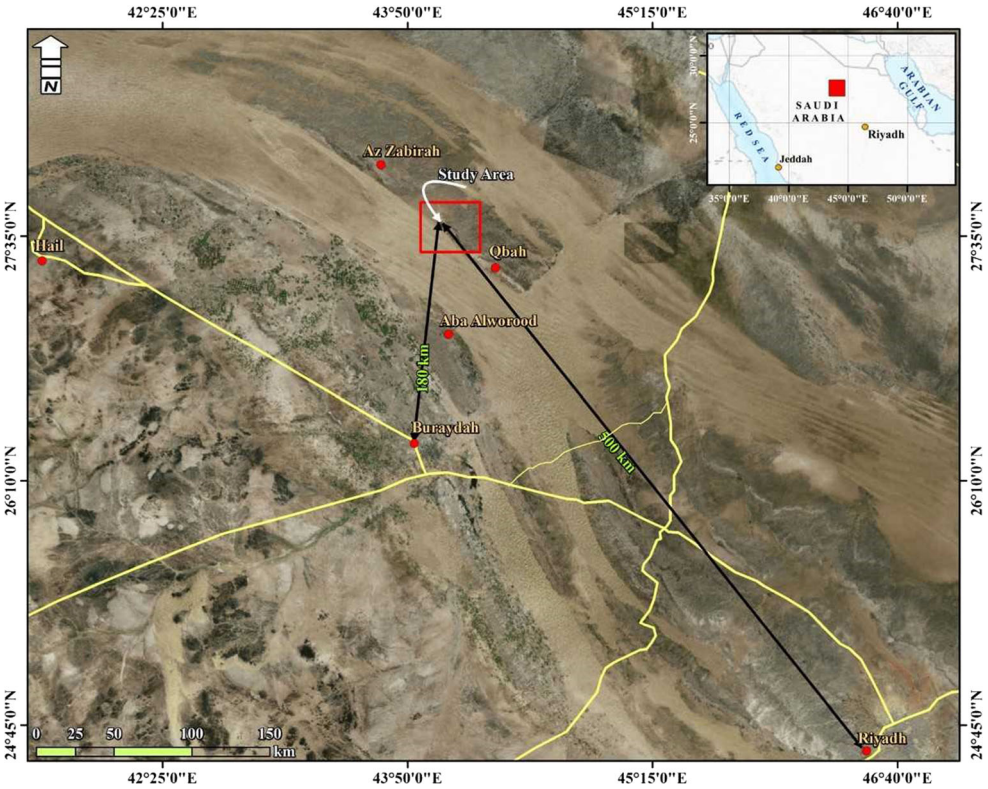

Fig. 1 Location map of study area (Yahya 2017)

for further geochemical and petrologic investigations. Thus, reflectance spectroscopy can play a significant role in identifying economically valuable deposits within surrounding rock based on absorption features in their respective reflectance profiles (Rao et al. 2017). According to Kumar et al. (2018), an 86% spectral absorption peak (at 2.27 μm) with 39.7 wt% Al_20_3 characterizes low-grade bauxites. The spectral signature of bauxite deposits with 80% spectral absorption could be classified as lateritic bauxite with 25.73 wt% Al_20_3, and 86% spectral absorption confirms association with Fe_2O_3 (at 0.91 μm).

Remote sensing using satellites has been applied with some success to bauxite exploration (Al-Jaf 2008; Satpathy et al. 2010; Kusuma et al. 2012; Guha et al. 2013; Rao et al. 2017; Babu et al. 2018; Lakshmi and Tiwari, 2018; Ouyang et al. 2019; Aravindan et al. 2020). The wavelength regions used for this have included the VNIR, SWIR, and thermal infrared (TIR). A mineralogical study of bauxite, iron, and kaolin in the western desert of Iraq was carried out by applying color composite, band ratio, and principal components analysis (PCA) techniques to Landsat 4, 5, and 7 satellite data as well as radar data (Al-Jaf 2008). Hyperspectral Hyperion data and multispectral Advanced Spaceborne Thermal Emission and Reflection Radiometer (ASTER) data were used for the mapping of bauxite deposits in Jharkhand, India (Satpathy et al. 2010; Kusuma et al. 2012; Guha et al. 2013). The VNIR and SWIR bands of the ASTER data were used in conjunction with the Shuttle Radar Topography Mission digital elevation model and field studies to quantify the mineralogical content of limestone- and bauxite-rich areas in southern India. A new approach to the spectral unmixing of ASTER image data allowed areas rich in carbonates and alumina to be delineated. ASTER data were used to delineate bauxite-rich pockets within laterites in Jharkhand, India (Guha et al. 2013), and band depth and simple ratio images were derived from ASTER data to map the spatial distribution of the bauxites developed within the lateritic province. Lakshmi and Tiwari (2018) applied spectral unmixing to the VNIR and SWIR bands of the ASTER data to detect and map the bauxite-rich zones in the Kolli Hills, Tamil Nadu, India. Verification of the results was performed by correlating the values obtained by unmixing. Linear spectral unmixing, mixture-tuned matched filtering, spectral-feature fitting, and spectral-angle techniques were applied to hyperspectral Hyperion data to map aluminum-rich laterites in India (Babu et al. 2018). The spatial distribution of potential bauxites on the Bolaven Plateau on the Indochina peninsula was investigated using a Boolean-modeling process within a geographic information system environment involving constraints such as rock, topographic features, and vegetation coverage (Ouyang et al. 2019). VNIR bands (1–4) of the ASTER data were used to distinguish bauxite deposits from the associated laterites in Salem District, Tamil Nadu, India (Aravindan et al. 2020). The results showed that the bauxite deposits are characterized by a strong absorption feature at 2.26 μm. The spectra for samples of different grades of bauxite match well the US

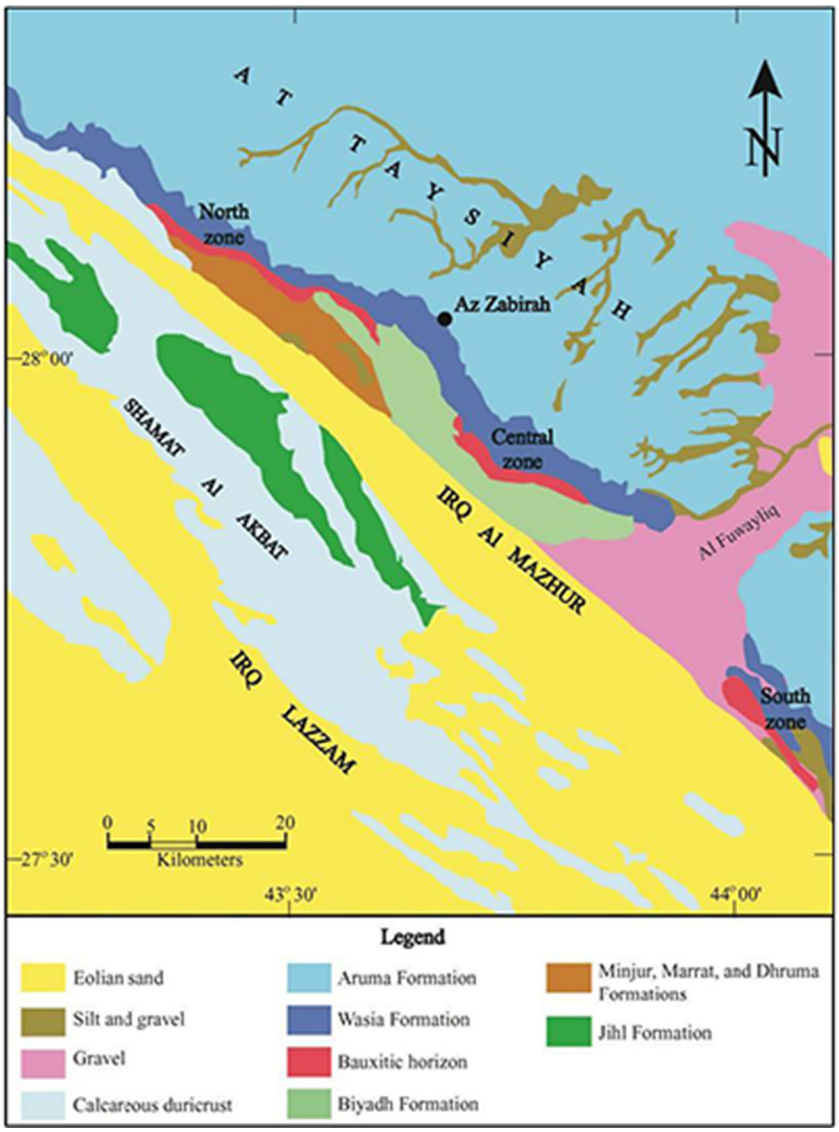

Fig. 2 Geological map of three zones containing bauxite deposits at Az Zabirah (Black et al. 1982)

Geological Survey (USGS) library spectra. The results also showed good correspondence between the convolved ASTER laboratory spectra of bauxite samples and bauxite pixels.

Most previous studies have focused on the geochemical, mineralogical, and petrological characteristics of bauxite deposits (Al-mutairi 2013; Yahya 2017; Al-mutairi 2019). Ground-penetrating radar has also been used to map lateritic bauxite (Al-mutairi et al. 2019). Apparently, our study is the first in which reflectance spectroscopy and remote sensing have been used for distinguishing bauxite deposits. Our objective was to use reflectance spectroscopy and ASTER data (in the range 0.4–2.5 μm) to identify bauxite deposits based on the spectral properties of the dominant minerals found in bauxite. We integrated the results of the reflectance spectroscopy with those obtained using X-ray diffraction (XRD). The results of this study will be of economic importance in hyper-arid environments such as in Saudi Arabia.

Study area and geologic setting

The Az Zabirah deposit (Lat 27° 55′ N, Long 43° 43′ E) lies within the Qasim region of Saudi Arabia, 150 km southwest of the trans-Arabian pipeline and 180 km north of Buraydah (Fig. 1). The study area is 580–650 m above sea level and is part of the cuesta region of Saudi Arabia. Differential erosion of the Mesozoic sedimentary sequence has produced a succession of northwest-trending escarpments separated by plains on dip slopes. The bauxite scarp is 1–10 m high and is extensively dissected.

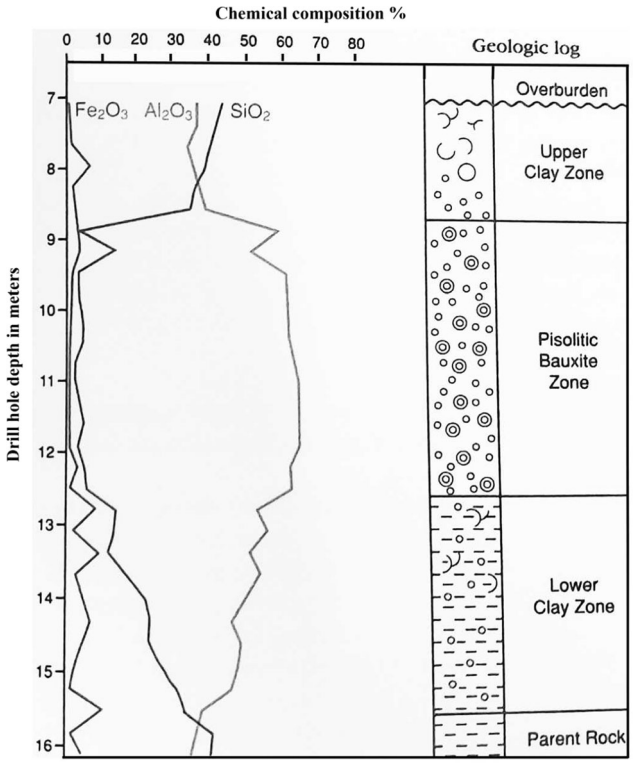

Fig. 3 Typical bauxite profile within study area. Profile includes overburden sandstone, upper clay zone (UCZ), pisolitic bauxite zone (BXZ), and lower clay zone (LCZ)

The bauxite occurs as an in situ paleolaterite profile above a regional Early Cretaceous unconformity and developed on a sequence of terrigenous clastic sedimentary rocks that dip at ~1° to the east–northeast.

Early Cretaceous sedimentary rocks, unconformably overlying Triassic–Jurassic beds, are present in the parent-rock sequence (Bowden 1981; Riofinex 1982, 1983). Bauxite (Bowden 1981; Riofinex Geological Mission 1982, 1983) is preserved beneath a series of fluviatile sandstone and lagoonal mudstones, with thin but extensive carbonate intercalations. This series is referred to as the overburden sequence and ranges in age from Early to Late Cretaceous. The overburden sequence has a regional dip of 1° to the northeast. Bauxite crops out in three main geographic areas (Fig. 2)—the northern, central, and southern zones—and is exposed discontinuously along a low scarp over a total strike length of 105 km. It dips gently to the northeast with conformable overlying strata. In the vicinity of Az Zabirah, the southern bauxite zone, which is 10 m thick, is further subdivided into three zones (Fig. 3): the lower clay zone (LCZ), the pisolitic bauxite zone (BXZ), and the upper clay zone (UCZ) (Black et al. 1982). Commercial bauxite deposits are limited to the BXZ and UCZ.

The Biyadh sandstone is within the Early Cretaceous rocks and outcrops in the southwestern part of the study area (Bowden 1981; Riofinex Geological Mission 1982, 1983).

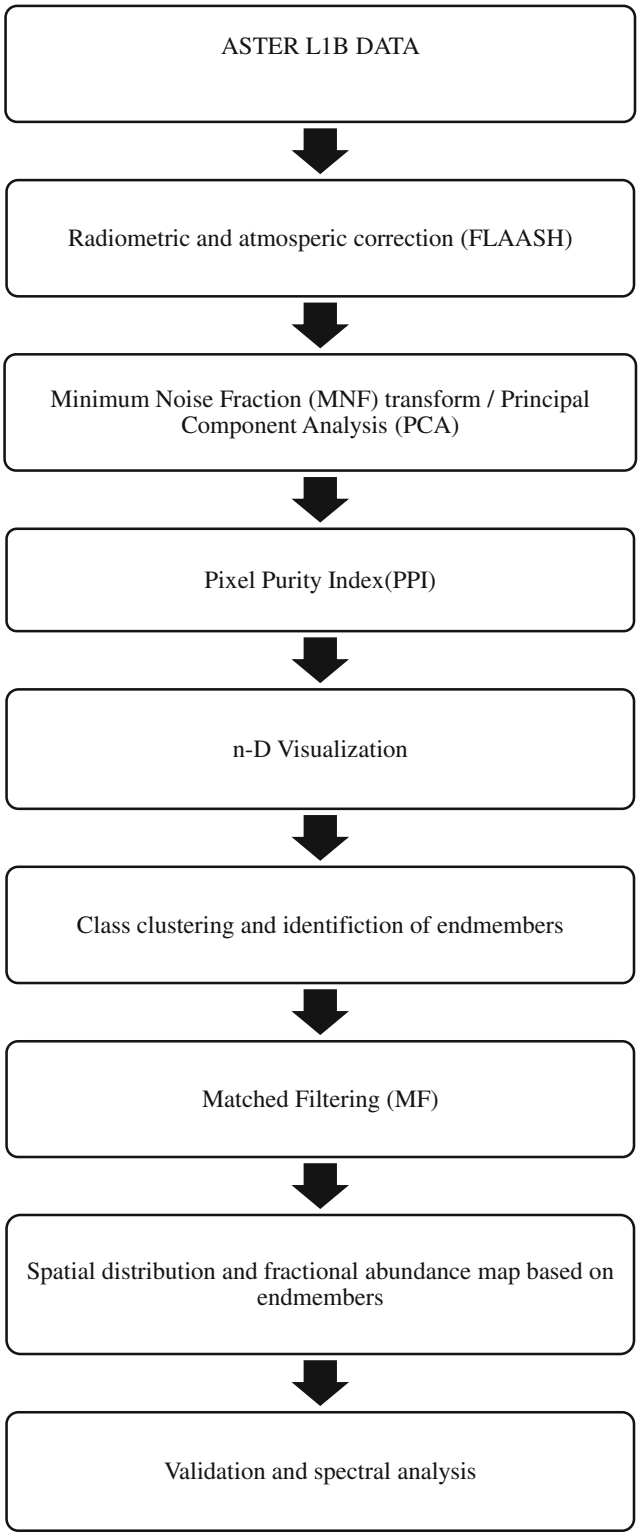

Fig. 4 Flowchart of methodology used in current study

The sandstone strikes northwest–southeast over a distance of ~3–11 km northwest of the village of Al Bi'ithah. The Biyadh sandstone is ~50 m thick and is composed of fine-grained, well-bedded sandstone.

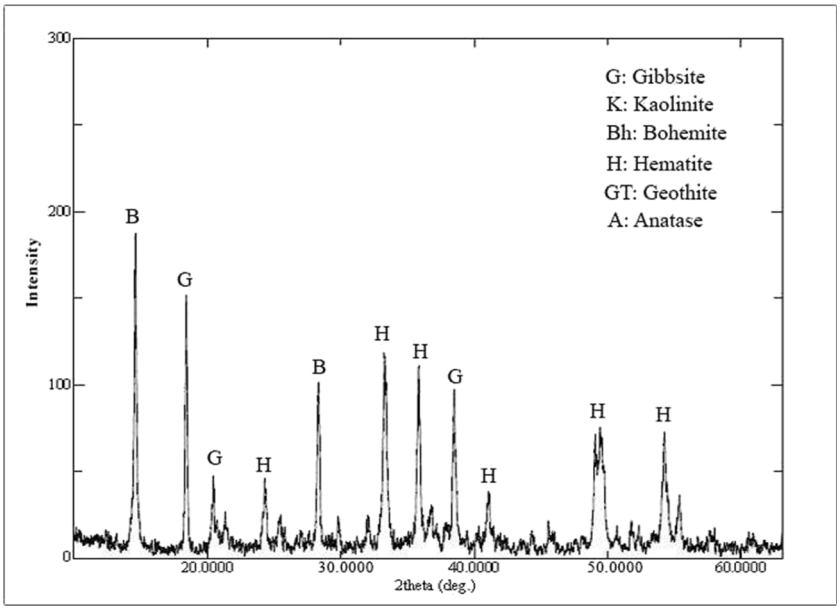

Fig. 5 X-ray diffraction (XRD) patterns of collected bauxite samples. Samples are composed of goethite, gibbsite, boehmite, kaolinite, hematite, and quartz

Methods

Fieldwork and sampling

Samples were collected at Az Zabirah from the bauxite profile, which includes UCZ, BXZ, LCZ, and overlying sandstone (Fig. 3). The geographic locations of the collected samples were obtained using a global positioning system handheld device. The samples were put into plastic bags and taken to the laboratory for further investigation.

Mineralogical analysis

The powdered bauxite samples were subjected to mineralogical analysis using XRD, at a fixed wavelength. A goniometer was used to record the intensity of the reflected radiation. The diffraction peaks were converted to d-spacings, and these were then compared with standard reference patterns to identify unknown minerals.

Laboratory spectral measurements

Laboratory reflectance spectra (0.315–2.519 μm) were obtained for all the collected bauxite samples using a Geophysical and Environmental Research Corporation GER 3700 spectrometer. The measurements made with the spectrometer required an external source of light (a 500-W halogen lamp). The distance between the sensor and the samples was ~25 cm, and the sensor was placed vertically above the samples. The GER 3700 has 640 bands and a ~100-cm^2 ground-level field

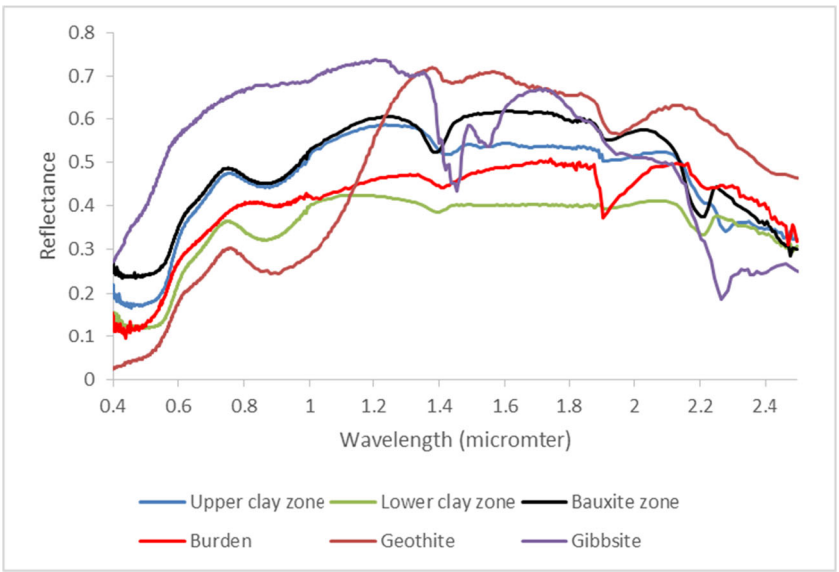

Fig. 6 U.S. Geological Survey (USGS) reflectance spectra of goethite, gibbsite, and kaolinite (Clark 1993) and Geophysical and Environmental Research Corporation GER 3700 spectrometer spectra of collected samples (0.4–2.5 μm)

of view. The mineralogical identification of the collected samples was accomplished by comparing the reflectance spectra of these samples with the spectra contained in the USGS mineral spectral library (Clark 1999).

Spectral analysis and image processing

According to Yamaguchi et al. (1998), ASTER data include 14 different spectral bands: three VNIR, six SWIR, and five TIR channels. The TIR region of the ASTER data was not considered in this study. The spatial resolution of the other bands ranges within 15–90 m. Cloud-free level 1B (L1B) ASTER data acquired on November 5, 2003, were used in this study, and image processing of these data was performed using Environment for Visualizing Images (ENVI) v.5.2 software. The SWIR bands of the ASTER data were processed using crosstalk-correction software to counteract the anomalously high radiance in bands 5 and 9 due to the transmission of energy from band 4 optical elements to the adjacent bands 5 and 9 detectors (Zhang et al. 2016). The ASTER VNIR bands, which have a spatial resolution of 15 m, were resampled to combine with the SWIR bands, which have a spatial resolution of 30 m, by using the cubic-convolution method. The three VNIR bands were then combined with the six SWIR bands to produce a nine-band ASTER image. Finally, the crosstalk-corrected nine-band ASTER image was calibrated to surface reflectance by using the Fast Line-of-Sight Atmospheric Analysis of Spectral Hypercubes atmospheric correction model, which incorporates the Moderate Resolution Transmittance radiation-transfer code, to remove the atmospheric attenuation and produce the reflectance imagery.

Different image-processing techniques were applied to determine the mineralogical composition of the bauxite deposits. The techniques that were applied included minimum noise fraction (MNF), pixel purity index analysis (PPI), n-D visualization, and matched filtering (MF) (Fig. 4).

MNF and PCA transformation methods (Green et al. 1998) were applied to the ASTER (L1B) data to estimate and remove noise, determine the information dimensionality of the imagery, and facilitate the subsequent computer processing and analyses. To isolate the purest or least-mixed images, PPI was run on the MNF images from the transformed datasets by projecting the MNF-transformed image spectra to random unit vectors until the most extreme pixels were counted and tallied (Boardman et al. 1999). The isolated spectra were then clustered into discrete PPI image endmember classes using n-D visualization (Boardman 1993; Boardman et al. 1999).

MF is a mapping technique used to determine abundances of user-defined endmembers by partial unmixing. It maximizes the response of a known endmember while suppressing the response of the composite unknown background (Stocker et al. 1990). The technique also provides a means of rapidly detecting specific minerals based on matches to specific library or image endmember spectra. MF results are presented as gray-scale images with values in the range 0.0–1.0 (where 1.0 is a perfect match); this provides a means of estimating the relative degree of matching to the reference spectrum.

Results and discussion

Mineralogical analysis

XRD indicated that the mineralogy of the bauxite deposits consists of gibbsite, boehmite, and goethite (Fig. 5); kaolinite, hematite, anatase, and quartz also are present in small amounts. The upper and lower clay zones are composed mainly of kaolinite, whereas quartz dominates the

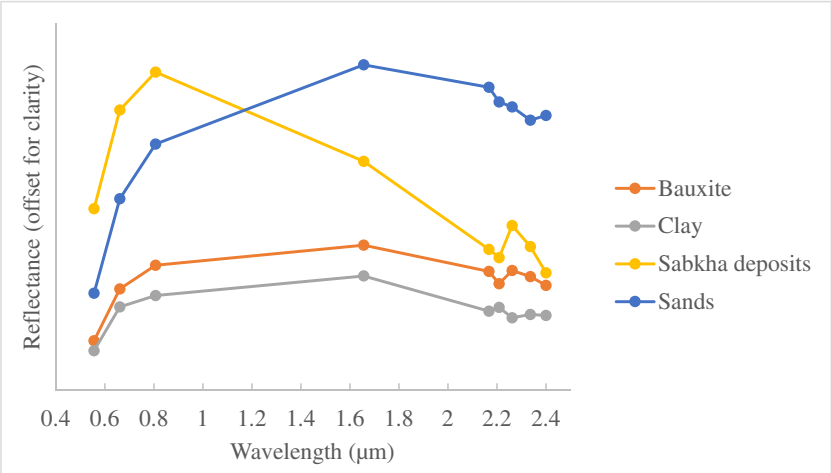

Fig. 7 Spectra of Advanced Spaceborne Thermal Emission and Reflection Radiometer (ASTER)-derived endmembers used in matched-filtering classification. Identified endmembers are bauxite, clay, sand, and sabkha deposits

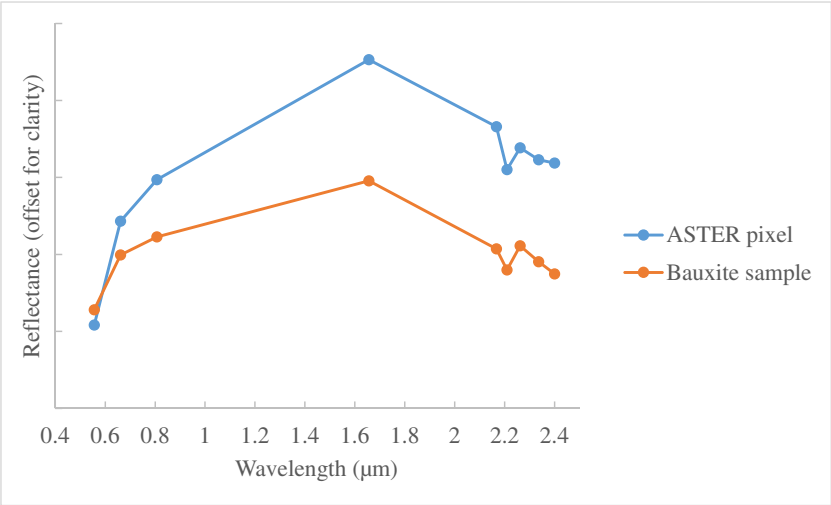

Fig. 8 Comparison of laboratory-derived bauxite spectrum with corresponding Advanced Spaceborne Thermal Emission and Reflection Radiometer (ASTER) pixels

overburden deposits. These results agree well with the findings of Yahya (2017) and Al-mutairi (2019).

Spectral analysis

The bauxite spectra and other components of the bauxite profile obtained using the GER 3700 spectroradiometer are shown in Fig. 6. The bauxite spectra exhibit strong Al–OH vibration features at wavelengths of 1.54, 2.26, and 2.35 μm and weak features at 0.48 and 0.99 μm. The absorption features near 0.50 and 0.68 μm are due to iron oxide. The absorption minima at 1.4 and 1.9 μm can be attributed to the presence of water. The bauxite deposits' VNIR absorption features (0.4–1.1 μm) are characteristic of the spectra of iron oxides (hematite) and hydroxides (goethite and gibbsite) (Hunt and Salisbury 1974; Hunt 1977; Hunt and Ashley 1979). These minerals exhibit charge transfer and Fe^{3+}-crystal field bands. The spectrum of hematite is dominated by different diagnostic absorption features at ~0.53, ~0.63, and ~0.87 μm. The spectrum of goethite is distinguished by absorption features at 0.48, 0.67, and 0.94 μm (Hunt et al. 1971). Multiple absorption features centered at 1.40 and 1.55 μm dominate the spectrum of gibbsite. The spectrum of kaolinite shows an Al–OH absorption feature near 2.165–2.20 μm (Hunt et al. 1971) and an absorption feature near 1.40 μm. The spectral reflectance curves of UCZ and LCZ are characterized by diagnostic absorption features in the SWIR wavelength region due to the presence of hydroxyl (OH) and water (H_2O) (Rowan et al. 2003). The spectra of the overburden deposits have higher reflectance values in the VNIR and SWIR regions and are characterized by absorption features at 2.2 μm (due to clay) and 2.33 μm (due to carbonates. The spectrum of gypsum from the sabkha deposits has the highest ASTER band 3 reflectance value, with a decline in reflectance in the VNIR and an absorption feature at 2.205 μm that is probably due to clay (Fig. 7).

Remote sensing data were used to detect and map bauxite deposits based on their spectral reflectance curves. The sharp fall in reflectance in ASTER band 4 data centered ~1.65 μm with a dip at ~0.55 μm (ASTER band 1) matches the spectral behavior of goethite (Fig. 7). The absorption feature at 2.26 μm (ASTER band 7) and the shoulders at 2.16 and

Table 1 Eigenvectors and eigenvalues obtained from principal components analysis (PCA) using correlation matrix

	Band 1	Band 2	Band 3	Band 4	Band 5	Band 6	Band 7	Band 8	Band 9
PCA1	0.04	0.19	0.26	0.37	0.40	0.38	0.39	0.39	0.39
PCA2	0.72	0.44	0.43	0.05	−0.08	−0.03	−0.15	−0.23	−0.13
PCA3	−0.42	0.38	0.45	−0.10	−0.36	−0.46	0.05	0.35	0.06
PCA4	−0.34	−0.01	0.16	0.79	0.00	−0.07	−0.15	−0.41	−0.21
PCA5	0.11	−0.07	−0.13	0.15	−0.38	−0.07	−0.25	−0.18	0.84
PCA6	0.33	−0.01	−0.42	0.41	−0.46	−0.16	0.35	0.36	−0.22
PCA7	0.16	0.02	−0.18	0.07	0.57	−0.77	0.09	−0.05	0.15
PCA8	−0.07	0.47	−0.39	0.11	0.17	0.11	−0.66	0.37	−0.06
PCA9	0.20	−0.63	0.38	0.13	0.04	−0.11	−0.42	0.45	−0.06

The bold values represent the high coefficients for each principal component

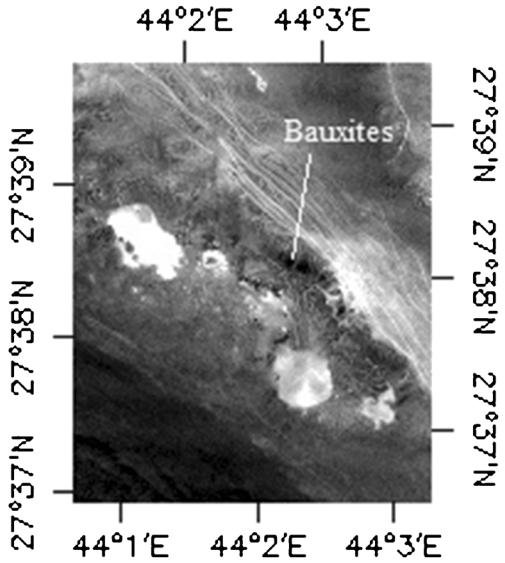

Fig. 9 Uncorrelated image bands (principal components band 2) extracted from Advanced Spaceborne Thermal Emission and Reflection Radiometer (ASTER) data. Bauxite is shown as black pixels, and the sabkha deposits are displayed in white pixels

2.33 μm (ASTER bands 5 and 8) are similar to the spectra of gibbsite. The general spectral shape of endmember bauxite deposits derived from ASTER closely corresponds to bauxite reference spectra (Fig. 8). The integration of remote sensing data with reflectance spectroscopy and XRD results thus is useful for providing information about the chemical composition of bauxite deposits. The use of these methods showed that the bauxite in the study area is composed of iron oxide and clay minerals.

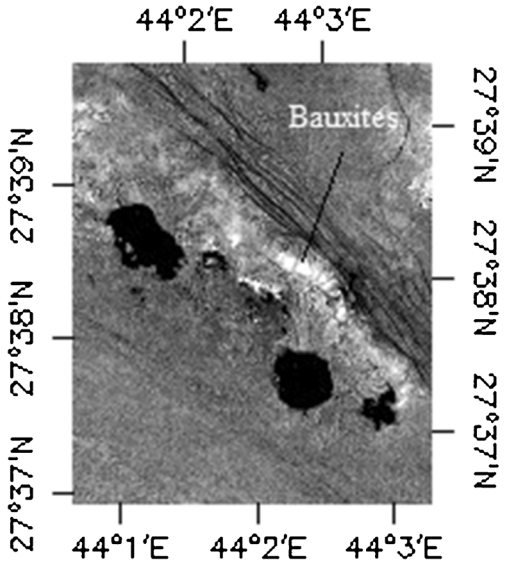

Fig. 10 Abundance (fraction) image for bauxite using Advanced Spaceborne Thermal Emission and Reflection Radiometer (ASTER) data. Bauxite is shown in white pixels

Mapping of bauxites

The eigenvectors and eigenvalues obtained from PCA using the correlation matrix are depicted in Table 1. Spatially coherent information is clearly observed in PCA bands 1–6. PCA bands 7–9 exhibit less variance and therefore commonly appear noisy.

The results demonstrate that PC1 has the highest variance (86.74%), with positive loadings for all spectra. According to Pour and Hashim (2011), the strong positive correlation among ASTER bands is due to overall scene brightness or albedo. The second highest proportion of variance (11%) is associated with PC2. Eigenvector loadings for PC2 differentiate between VNIR and SWIR bands. This component includes most of the spectral information from bands 1–3. The PCA results reveal that PC2 is the best of all the components for highlighting the extent of bauxite deposits in the study area (Fig. 9). The bauxite deposits' spatial distribution represented in the PC2 image agrees well with field observations for the collected samples and with the geologic map of the study area. The spectral features of iron oxide minerals are expressed in ASTER bands 1–3. The PC2 results showed that the highest spectral contrast was recorded between bands 1 and 3.

The MF method was applied to the ASTER data to produce images showing the spatial distribution and abundances of the bauxite deposits in the study area (Fig. 10). Brighter pixels in the RGB images represent higher abundances of bauxite. Mixed colors in these images represent pixels that contain mixtures of endmember classes. Overall, the integration of ASTER data, multi-image processing methods including MF and PCA, spectroscopic measurements, mineralogical analyses, and field observations proved to be effective for the mapping of bauxite deposits in arid and semiarid environments.

Conclusions

Reflectance spectroscopy and ASTER data were found to be effective in detecting and mapping bauxite deposits in the area in and surrounding the town of Az Zabirah in north-central Saudi Arabia. Reflectance spectroscopy yielded mineralogical and chemical compositions of the collected samples, which were found to be mainly composed of goethite, gibbsite, and boehmite. The spectral signatures in the VNIR region proved to be useful for establishing the abundance of iron oxide/hydroxide minerals (such as goethite and hematite) in the bauxite deposits. Exploration for kaolinite and gibbsite was possible using SWIR data (2.160–2.265

μm). The general spectral shape of bauxite deposits endmember derived from ASTER closely matches bauxite reference spectra. PC2 was the best component for distinguishing bauxite deposits in the study area. MF provided a rapid means of identifying specific materials based on matches to library or image endmember spectra and did not require knowledge of all the endmembers within an image scene. The PCA and MF techniques can thus be used to identify economically valuable minerals in arid and semiarid environments.

Funding This Project was funded by the KSU National Plan for Science, Technology and Innovation (NPST), Award Number (14-SPA686-02).

Declarations

Competing interests The authors declare that they have no competing interests.

References

Al-jaf A (2008) Remote sensing and GIS for studying some geological phenomena and mineral deposits in the western Desert in IRAQ. Master thesis submitted to the College of Science University of Baghdad.

Al-mutairi A (2013) Mineralogy and geochemistry of bauxite ore deposits at Az Zabirah Area. In: Central Northern of Saudi Arabia. Master thesis submitted at the Department of Geology and Geophysics. College of Science, King Saud University, Saudi Arabia

Al-mutairi NB (2019) Geologic setting of Az Zabirah south zone bauxite ore deposits, Central North of Saudi Arabia. Thesis Master Submitted to the Department of Geology and Geophysics. College of Science, King Saud University, Saudi Arabia

Al-mutairi YA, El-Araby HM, Ghrefat HA, Alotaibi AM (2019) Mapping lateritic bauxite deposits at Az Zabirah, Saudi Arabia, using ground-penetration radar exploration method. Arab J Geosci 12:347

Aravindan S, Bharathiraja S, Kumar BS (2020) Hyper spectral signature and ASTER data analysis for mapping of Bauxite deposits in Shevaroy hill of Tamil Nadu, India. Int Res J Earth Sci 8(1):13–19

Babu RMJ, Rao DEN, Kallempudi L, Das Iswar C (2018) Mapping of aluminous rich laterite depositions through hyper spectral remote sensing. Int J Geosci 9:93–105

Black RY, Bognar B, Watson AD, Barnes DP (1982) Evaluation of the Az Zabira bauxite deposit (1980-1982). Riofinex Ltd. Tech. Rep

Boardman JW (1993) Automated spectral unmixing of AVIRIS data using convex geometry concepts: In Summaries, Fourth JPL Airborne Geoscience Workshop, JPL Publication 93-26, 1:11-14

Boardman JW, Kruse FA, Green R (1999) Mapping target signatures via partial unmixing of AVIRIS data: In Summaries, Fifth JPL Airborne Earth Science Workshop, JPL Publication 95-1, 1:23-26

Bowden RA (1981) Geology of the Az Zabira bauxite occurrence. Riofinex Ltd., open file report

Chang CW, Laird DA, Mausbach MJ, Hurburgh CRJ (2001) Near-infrared reflectance spectroscopy - principal components regression analyses of soil properties. Soil Sci Soc Am J 65:480–490

Clark RN (1999) Spectroscopy of rocks and minerals; principles of spectroscopy. Remote sensing for earth science. In: Manual of remote sensing. Wiley, NJ

Clark RN (2011) Spectroscopy of rocks and minerals, and principles of spectroscopy. In: Manual of remote sensing. Wiley, NJ

Clark RN, Swayze GA, Gallagher A, King TVV, Calvin WM (1993) The U.S. Geological Survey digital spectral library, version 1: 0.2 to 3.0 μm: U.S. Geological Survey Open-File Report 93-592, p 1340

Fahad M, Iqbal Y, Ubic R (2009) Bauxite deposits in Pakistan: an introduction. J Pak Mater Soc 3

Green RO, Eastwood ML, Chrien TG, Aronsson M, Chippendale BJ, Faust JA, Pavri BE, Chovit CJ, Solis M, Olah MR, Williams O (1998) Imaging spectroscopy and the airborne visible/infrared imaging spectrometer (AVIRIS). Remote Sens Environ 65:227–248

Grove CI, Hook SJ, Paylor (eds) (1995) Laboratory reflectance spectra of 166 minerals 0.4 to 2.5 micrometer. Jet Propul Laboratory (JPL) Publ. 92-2. California Institute of Technology, Pasadena

Guha A, Singh VK, Parveen R, Kumar KV, Jeyaseelan AT, Dhanamjaya Rao EN (2013) Analysis of ASTER data for mapping bauxite rich pockets within high altitude lateritic bauxite, Jharkhand, India. Int J Appl Earth Obs Geoinf 21:184–194

Hunt GR (1977) Spectral signatures of particulate minerals in the visible and near infrared. Geophysics 42:501–513

Hunt GR, Ashley RP (1979) Spectra of altered rocks in the visible and near infrared. Econ Geol 74:1613–1629

Hunt GR, Salisbury JW (1974). Mid-infrared spectral behavior of igneous rocks, AFCRL-TR-0625

Hunt GR, Salisbury JW, Lenhoff CJ (1971) Visible and near-infrared spectra of minerals and rocks: IV. Sulphides and sulphates. Mod Geol 3:1–14

Kumar KS, Aravindan S, Bharathiraja S (2018) Hyper spectral signature and geochemical study of Eastern Ghat bauxite in the part of Kollimalai, Namakkal District, Tamil Nadu, India. IJSRR 7(4): 1784–1793

Kusuma KN, Ramakrishnan D, Pandalai HS (2012) Spectral pathways for effective delineation of high-grade bauxites: a case study from the Savitri River Basin, Maharashtra, India, using EO-1 Hyperion data. Int J Remote Sens 33:7273–7290

Lakshmi V, Tiwari R (2018) Mapping of bauxite ore using remote sensing and GIS. Int J Pure Appl Math 119:3367–3375

Ouyang Y, Liu H, Wang X, Liu S, Zhang J, Gao H (2019) Spatial distribution prediction of laterite bauxite in Bolaven Plateau using GIS. J Earth Sci 30(5):1010–1019

Pour AB, Hashim M (2011) Application of Advanced Spaceborne Thermal Emission And Reflection Radiometer (ASTER) data in geological mapping. Int J Phys Sci 6(33):7657–7668

Rao AD, Guha A, Kumar VK, Rao D (2017) Potentials of spectrometry in economic rocks mapping -a brief analysis for three economic rocks of three different geological provinces of India. J Remote Sens GIS 6:4

Riofinex (1982) Evaluation of the Az Zabirah bauxite deposit, Plate 3, Az Zabirah bauxite prospect, South Zone geology, 1:50 000: Ma'aden data base, Riyadh

Riofinex (1983) Factors relating to the development of a bauxite mine at Az Zabirah - an order of magnitude study, Saudi Arabian Directorate General of Mineral Resources: Confidential Report RF-CR-03-1 - Ma'aden data base, Riyadh

Rowan LC, Hook SJ, Abrams MJ, Mars JC (2003) Mapping hydrothermally altered rocks at cuprite, Nevada using the Advanced Spaceborne Thermal Emissivity and Reflection Radiometer ASTER. A new satellite-imaging system. Econ Geol 98:1019–1027

Satpathy R, Singh VK, Parveen R, Jeyaseelan AT (2010) Spectral analysis of Hyperion data for mapping the spatial variation of AL+OH minerals in a part of Latehar and Gumla District, Jharkhand. J Geogr Inf Syst 2:210–214

Stocker AD, Reed IS, Yu X (1990) Multidimensional signal processing for electrooptical target detection. Proc Soc Photo Opt Instrum Eng International Society for Optical Engineering (1305)

Thompson AJB, Hauff PL, Robitaille AJ (1999) Alteration mapping in exploration: application of short-wave infrared (SWIR) spectroscopy. SEG Newsl 39:16–27

Valeton I (1972) Bauxites. Elsevier, New York

Yahya MMA (2017). Petrological, paleoclimatic and geologic setting of Az Zavirah Bauxite ore deposits, Central North of Saudi Arabia. Master Thesis Submitted to the Department of Geology and Geophysics. Saudi Arabia: College of Science, King Saud University

Yamaguchi Y, Kahle A, Tsu H, Kawakami T, Pniel M (1998) Overview of Advanced Spaceborne Thermal Emission and Reflection Radiometer (ASTER). IEEE Trans Geosci Remote Sens 36:1062–1071

Zhang T, Yi G, Li H, Wang Z, Tang J, Zhong K, Li Y, Wang Q, Bie X (2016) Integrating data of ASTER and landsat-8 OLI (AO) for hydrothermal alteration mineral mapping in Duolong Porphyry Cu-Au deposit, Tibetan Plateau, China. Remote Sensing 8(11):890. https://doi.org/10.3390/rs8110890